PAPER

Particle-in-cell simulations of asymmetric reconnection driven by laser-powered capacitor coils

IOP Publishing Plasma Physics and Controlled Fusion
Plasma Phys. Control. Fusion **63** (2021) 015010 (10pp) https://doi.org/10.1088/1361-6587/abc600

Particle-in-cell simulations of asymmetric reconnection driven by laser-powered capacitor coils

Kai Huang[1,2], Quanming Lu[1,2], Abraham Chien[3], Lan Gao[3], Hantao Ji[3,4], Xueyi Wang[5] and Shui Wang[1,2]

[1] CAS Key Lab of Geospace Environment, Department of Geophysics and Planetary Science, University of Science and Technology of China, Hefei 230026, People's Republic of China
[2] CAS Center for Excellence in Comparative Planetology, Hefei 230026, People's Republic of China
[3] Princeton Plasma Physics Laboratory, Princeton University, Princeton, NJ 08543, United States of America
[4] Department of Astrophysical Sciences, Princeton University, Princeton, NJ 08544, United States of America
[5] Physics Department, Auburn University, Auburn, AL 36849, United States of America

E-mail: qmlu@ustc.edu.cn

Received 18 July 2020, revised 25 October 2020
Accepted for publication 29 October 2020
Published 20 November 2020

Abstract

During magnetic reconnection, such as in the magnetopause of magnetized planets, the upstream plasma conditions between the two inflow regions are usually different. In this paper, we demonstrate that such a kind of asymmetric reconnection can be studied in the laboratory using the recently proposed experimental scheme where reconnection is driven by laser-powered capacitor coils. Two-dimensional particle-in-cell simulations on the (z, r) plane in a cylindrical coordinate are conducted to study magnetic reconnection with the inflow along the r direction. Magnetic reconnection is found to be asymmetric with a stronger magnetic field in the inner (small r) inflow region and a weaker magnetic field in the outer (large r) inflow region due to the cylindrical symmetric geometry. Electron crescent velocity distributions are observed near the flow stagnation point while ion crescent velocity distributions are observed in the region with Larmor electric field. The out-of-plane Hall magnetic field is asymmetric between the two inflow regions with a larger spatial scale in the outer inflow region. This asymmetric Hall magnetic field configuration is different from that in previous studies. The typical reconnection rate increases with a stronger driver and the highest rate is around $0.2V_AB_0$, where B_0 is the typical value of the magnetic field and V_A is the Alfven speed. This study provides a new method to experimentally study asymmetric reconnection in the laboratory and has potential applications regarding magnetic reconnection in the magnetopause of magnetized planets.

Keywords: magnetic reconnection, asymmetric reconnection, Hall magnetic field, crescent distribution, particle-in-cell simulation, laser-powered capacitor coil

(Some figures may appear in color only in the online journal)

1. Introduction

Magnetic reconnection is a fundamental physical process that converts magnetic energy to plasma kinetic and thermal energy by rearranging the magnetic topology. It is believed to be responsible for the energy release phenomena in many space and astrophysical plasma environments, such as solar flares [1], magnetosphere substorms [2], sawtooth crashes in tokamaks [3], and gamma-ray bursts associated with supernovae [4]. Reconnection in the magnetopause of magnetized

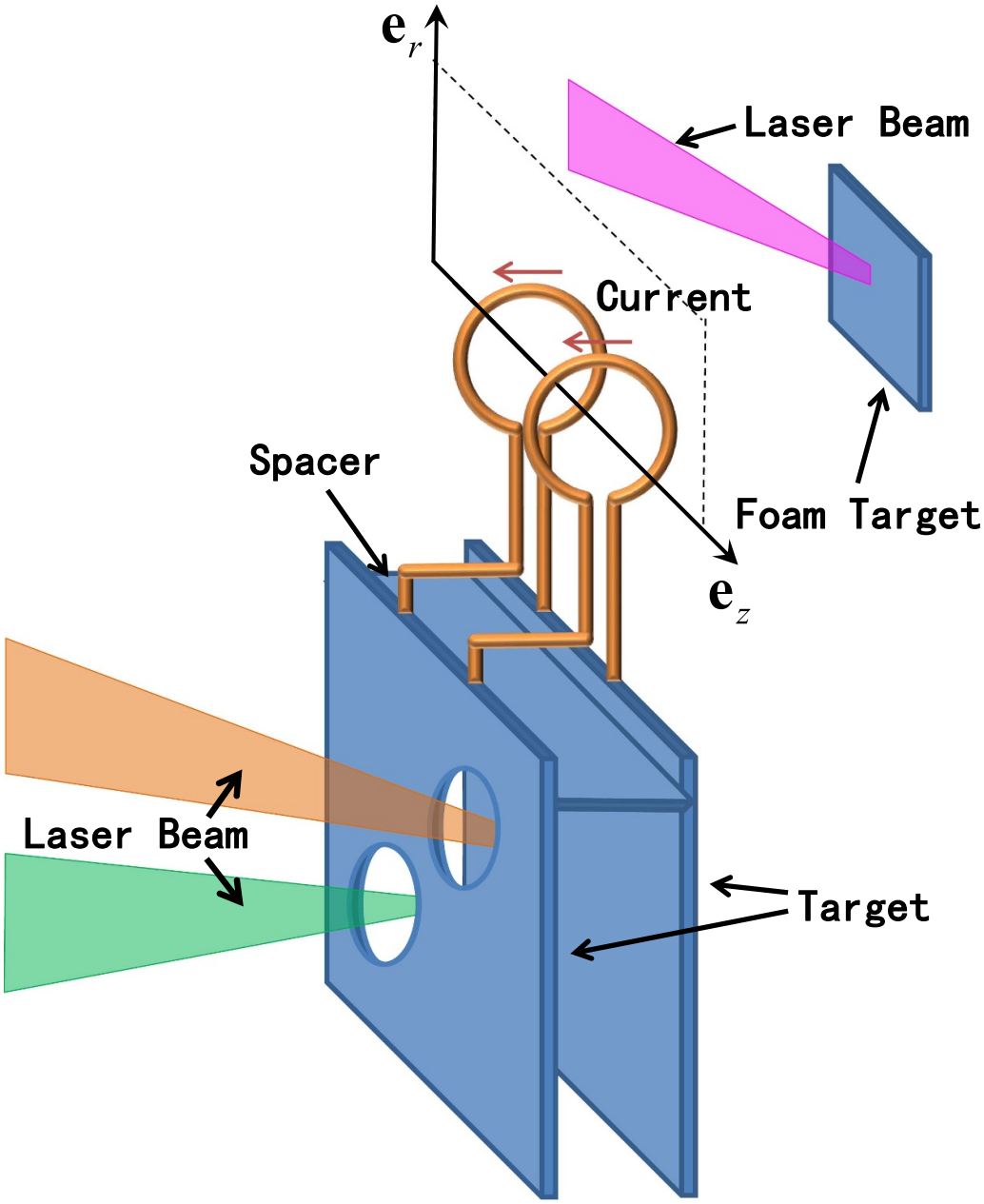

Figure 1. Sketch of magnetic reconnection driven by laser-capacitor coil. The dashed box with coordinate corresponding to the simulation domain. Reproduced from [18], with the permission of AIP Publishing.

planets is usually asymmetric where the upstream magnetic field, plasma density, or temperature is different between the two inflow regions. Many features of asymmetric reconnection such as the separated magnetic null point and flow stagnation point, asymmetric Hall magnetic field, and electron crescent velocity distributions have been observed by the Magnetospheric Multiscale Mission (MMS) and in some simulations [5–7].

Besides satellite observations and numerical simulations, experimental study of asymmetric reconnection using a high power laser in the laboratory has also been realized recently. Rosenberg *et al* [8] studied asymmetric driven reconnection in high-energy density plasma on OMEGA. Reconnection in their experiment occurs between two laser-produced plasma bubbles with a self-generated magnetic field. By introducing a time delay between two laser beams, the properties of the generated plasma bubbles will be different, leading to asymmetric reconnection. Similar experiments have also been conducted to study symmetric reconnection [9–11]. However, the plasma beta in these experiments is usually large and around 10, and the driving speed is much larger than the Alfven speed and the sonic speed. While in many astrophysical environments, such as Earth's magnetopause, the plasma beta is around or below one and the driving speed is not very large. To study reconnection in the low plasma beta condition, a new experimental scheme to fulfill reconnection using a laser-powered

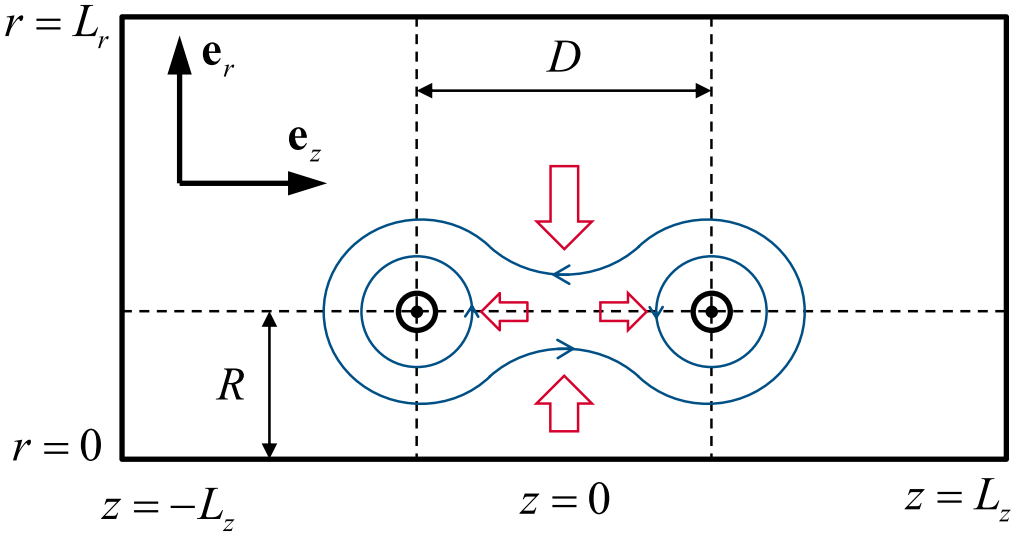

Figure 2. Sketch of half of the simulation domain and magnetic reconnection. Blue curves with arrow represent the magnetic field lines, while the red arrows show the reconnection inflow and outflow direction.

Table 1. Experimental parameters estimated by Chien *et al* [13].

Quantities	Estimated by Chien *et al* [13]
Ion species	Cu
Average ion charge Z	29
Electron density n_0	$10^{18}\,\mathrm{cm}^{-3}$
Ion density n_i	$3.45 \times 10^{16}\,\mathrm{cm}^{-3}$
Temperature T	500 eV
Typical magnetic field B_0	38 T
Radius of the coil R	300 μm
Distance between coils D	600 μm
Ion inertial length d_i	337 μm
Electron plasma beta β_e	0.14
Reverse ion gyrofreqency Ω_i^{-1}	0.6 ns
Current decay time T_D	8.6 ns

capacitor coils is proposed [12, 13]. A sketch of the experiment is shown in figure 1. Two laser beams are focused to the back target through the hole in the front target. Electrons with a high temperature will be generated from the back target and hit the front target. Strong currents are driven in the two parallel coils connected to the target due to the voltage between the two targets. A magnetic field is generated around the coils through Ampere's law. Experiments show that the magnetic field generated by this method can reach a kilotesla [14–17]. There is a spacer between the coils and the target to prevent the laser-produced high-energy plasma from affecting reconnection, the reconnection plasma is generated by irradiating another laser beam to a foam target. In this setup, the plasma beta can reach a low value ($\sim$0.1).

A previous study indicated that the current in the coils first increases after the laser irradiated on the target, and then decays [19]. During the increase phase of the coil current, the magnetic bubbles generated by the coil current expand and the reconnection inflow is along the z direction, reconnection is in the 'push phase' which has been studied using 2D particle-in-cell (PIC) simulations [18]. During the decay phase of the coil current, the magnetic bubbles contract and the reconnection inflow is along the r direction, reconnection is in the 'pull phase' [20]. In this paper, we focus on the pull phase of magnetic reconnection. Due to the cylindrical symmetric geometry, the upstream magnetic field is stronger in the inner inflow region (inside the ring-shaped coils) and weaker in the outer inflow region (outside the ring-shaped coils). Therefore magnetic reconnection will proceed in an asymmetric fashion. 2D PIC simulations are conducted to study such a kind of reconnection. Since the laser experiment is very expensive, it is hard to conduct it repeatedly. PIC simulation can provide guidances on parameters and diagnoses for experiments. It is also helpful for gaining a better understanding of the experimental results, because the diagnostic techniques are still limited in spatial and temporal resolutions. The simulation model is described in section 2. The simulation results are presented in section 3. Finally, in section 4, we summarize the conclusions and discuss the potential applications of this work.

2. Simulation model

The simulations in this work use the curvilinear coordinate fully electron and fully kinetic ion code (GCPIC) [18, 21]. Due to the cylindrical symmetric geometry of the experiment setup, our simulation is conducted on the (z, r) plane of the cylindrical coordinate where $\partial/\partial\theta = 0$ is satisfied for all quantities. The particle motion is solved in Cartesian coordinate, while the electromagnetic field is solved in cylindrical coordinate. The simulation parameters are designed to be comparable to the experimental parameters estimated by Chien *et al* [13] listed in table 1. Magnetic field is normalized to B_0 which is defined by $2\pi RB_0 = \mu_0 I_0$, where I_0 is the peak current in the coil and R is the radius of the coil, and μ_0 is the permeability of vacuum. The initial plasma density is uniform,

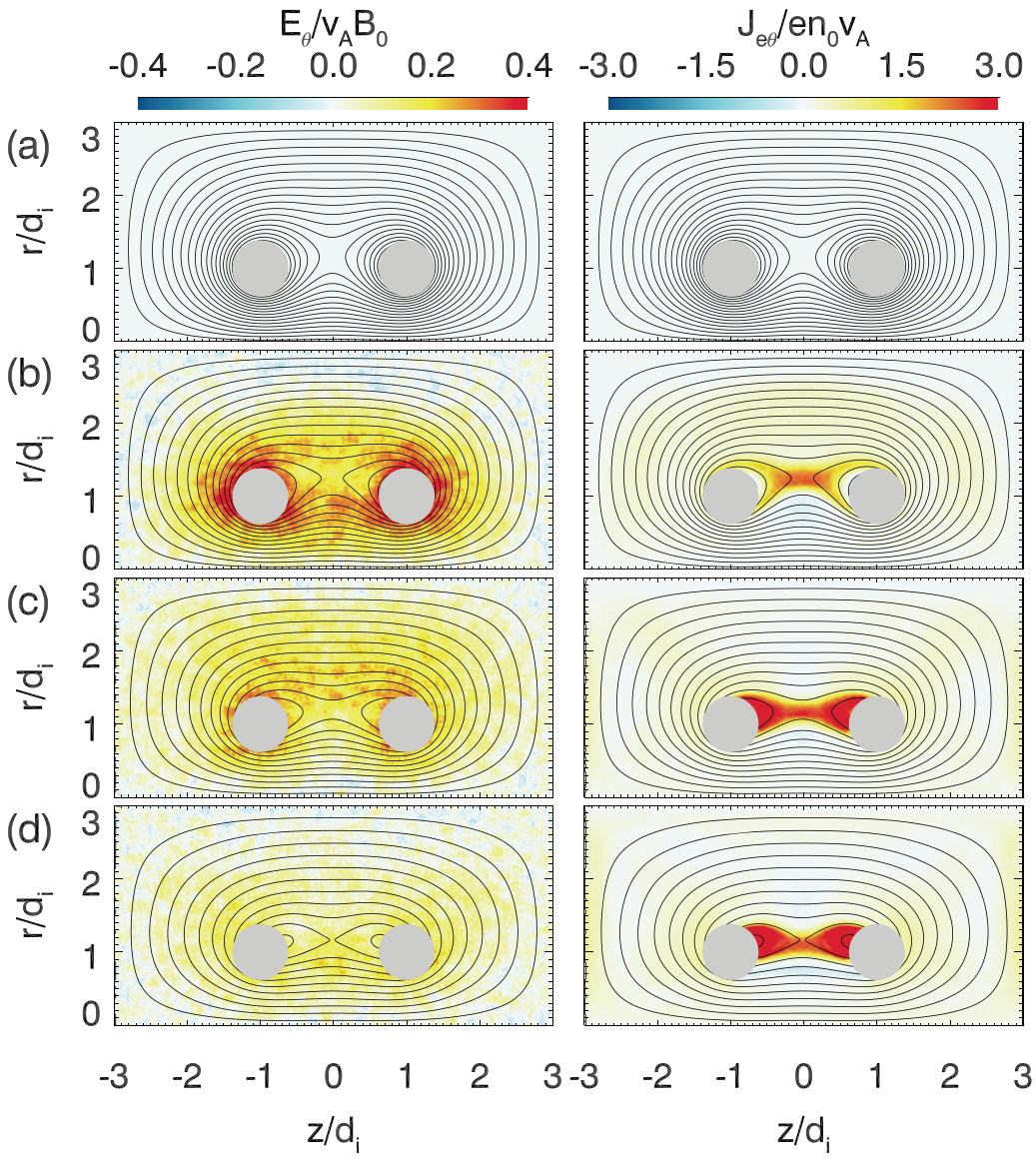

Figure 3. (a) Out-of-plane electric field E_θ/V_AB_0 and (b) out-of-plane electron current density $J_{e\theta}/en_0V_A$ at $\Omega_i t = 0$, 1, 2, and 3 respectively. The black curves represent the in-plane magnetic field lines. The decay time of the coil current is $\Omega_i T_D = 2$.

and the electron density is n_0. Ion to electron mass ratio is set to be $m_i/(Zm_e) = 100$ and ion density is $n_i = n_0/Z$, where Z is the average charge number of ions. Electron plasma beta is $\beta_e = 0.18$ while ion temperature is equal to electron temperature. Light speed is $c = 20\,V_A$, where $V_A = B_0/\sqrt{\mu_0 n_i m_i}$. The size of the simulation domain is $[-L_z, L_z] \times [-L_r, L_r]$ with spatial resolution $\Delta z = \Delta r = 0.015 d_i$, where $L_z = L_r = 3d_i$ and d_i is the ion inertia length defined by m_i and n_i. The time step is $\Delta t = 0.0002\,\Omega_i^{-1}$ and $\Omega_i = ZeB_0/m_i$ is the ion gyro frequency. Half of the simulation domain and a sketch of magnetic reconnection in the simulation plane are shown in figure 2. The position corresponding to the coils is set to be $z_c = \pm D/2$, $r_c = \pm R$, where the radius of the coil is $R = 1d_i$ and the distance between two coils is $D = 2d_i$. The cross section of the coil is assumed to be circular with a radius equal to $0.15d_i$. During the simulation, external driving current is applied on the grids corresponding to the cross section of each coil. The electromagnetic field is advanced using the sum of external current and current carried by particles while particle motion has no feedback on the external current. The initial current in the coil is I_0, and it decays with time following $I(t) = I_0 \exp(-t/T_D)$, where T_D is the decay time of the coil current. In the main case, $T_D = 2\,\Omega_i^{-1}$, we also study the effect of T_D on reconnection by changing T_D to 4, 6, 8, and 10 Ω_i^{-1}. Perfect conducting boundaries are used for field and reflecting boundaries for particles at both the r and z directions. Absorbing boundaries are set around the four coils to prevent the accumulation of particles near the coils. When the distance between the position of a particle (z_p, r_p) and the position of one coil (z_c, r_c) is less than $0.3d_i$, this particle will be absorbed. In all cases, 400 simulation particles per species are used in each grid.

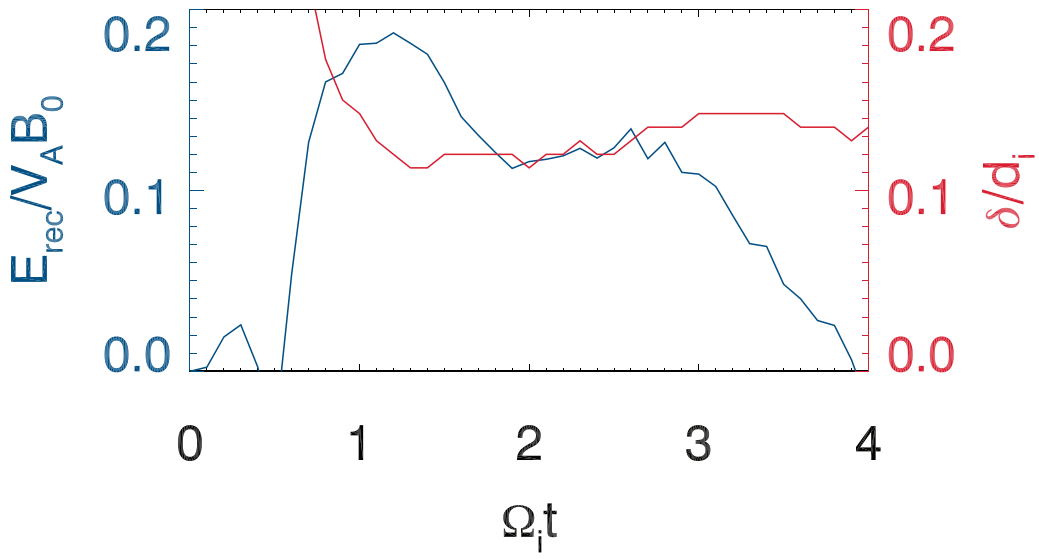

Figure 4. Time evolution of the reconnection rate E_{rec} and the half thickness of the current sheet δ along $z = 0$. The decay time of the coil current is $\Omega_i T_D = 2$.

3. Simulation results

Figure 3 shows the out-of-plane electric field $E_\theta / V_A B_0$ and the out-of-plane electron current density $J_{e\theta} / en_0 V_A$ at $\Omega_i t =$ 0, 1, 2, and 3, respectively. The black curves represent the in-plane magnetic field lines. The regions near the coils where the particles are absorbed are covered by gray discs. The initial magnetic field is generated by the current in the coil, $\nabla \times \mathbf{B} = \mu_0 J_{coil}$. With the decay of the current in the coils, the strength of the magnetic field decreases. As a result, an out-of-plane electric field is induced through Faraday's law $\nabla \times \mathbf{E} = -\partial \mathbf{B} / \partial t$. Plasmas will move to the coil region under the $\mathbf{E} \times \mathbf{B}$ drift with the magnetic field lines, resulting in the contracting of the magnetic bubbles. In the region near the magnetic null point between the two coils, the motion of electrons is decoupled with the magnetic field. A thin current sheet carried by electrons is formed in this region, and then magnetic reconnection occurs. Figure 4 shows the time evolution of the reconnection rate E_{rec} and the half thickness of the current sheet δ along $z = 0$. The reconnection rate is calculated by $E_{rec} = \partial \Phi_{rec} / \partial t$, where Φ_{rec} is the reconnected magnetic flux. The reconnection rate grows rapidly during $\Omega_i t =$ 0–1, along with the current sheet thinning. At around $\Omega_i t = 1$, the reconnection rate reaches the peak value close to 0.2, and the half thickness of the current sheet reaches the electron inertial length $d_e = 0.1 d_i$.

Figure 5 shows the magnetic field B_z / B_0 in (a), the electron bulk velocity V_{er} / V_A in (b), and the electric field $E_r / V_A B_0$ in (c), panel (d) plots the line cut of B_z, V_{er}, and E_r along $z = 0$ (the dashed line in panel (a) to (c)), the time is chosen to be $\Omega_i t = 3.0$. We find these quantities present asymmetric signatures between the outer and inner inflow regions. The amplitude of B_z in the inner inflow region (inside the ring-shaped coils) is about twice as large as that in the outer inflow region (outside the ring-shaped coils). This difference is formed due to the cylindrical symmetric geometry, and magnetic field will be stronger in the inner inflow region. As a result of the flux conservation during reconnection, the inflow speed V_{er} is larger in the outer inflow region, as shown in panel (b). Due to the different V_{er} in the two inflow regions, the stagnation point of the electron flow is separated from the magnetic null point (or X point). As shown in panel (d), the stagnation point of the electron flow is at $r \approx 1.0 d_i$, while the magnetic null point is located at $r \approx 1.2 d_i$. The bipolar Hall electric field E_r pointing to the reconnecting current sheet is also asymmetric and E_r in the inner inflow side is larger. At $r \approx 0.4 d_i$ to $0.8 d_i$ in panel (d), there is a region with E_r pointing in the the opposite direction from the Hall electric field in the inner inflow side. This is the Larmor electric field formed due to the finite Larmor radius effect of ions [22]. These features are consistent with previous simulations of asymmetric reconnection in a Harris sheet [7], as well as the satellite observations of magnetopause reconnection.

Figure 6 shows the distribution function of electrons and ions at $\Omega_i t = 3.0$. Panels (a) to (c) show the electron distribution in rectangular boxes centered on $z / d_i = 0$, $r / d_i =$ 1.0875, 1.0125, and 0.9375 respectively, close to the stagnation point of electron flow. Panels (d) to (f) show the ion distribution in rectangular boxes centered on $z / d_i = 0$, $r / d_i =$ 0.825, 0.675, and 0.525 respectively, close to the region with the Larmor electric field. Electron distribution function is calculated by accumulating electrons in a $0.3 d_i \times 0.075 d_i$ box in the $z - r$ plane, while a $0.3 d_i \times 0.15 d_i$ box is used for ions. All the distribution functions are shown in $v_\theta - v_r$ space and have been integrated over v_z. We can find that the electron distribution has two components, a core component with nearly Maxwell distribution and a crescent-shaped component surrounding the core component. It is similar to that observed by MMS in the electron diffusion region (EDR) encounter during magnetopause reconnection [5]. In panel (a), the crescent component is hard to distinguish, while in panels (b) and (c), the crescent component is very clear. From panel (b) to (c), the position

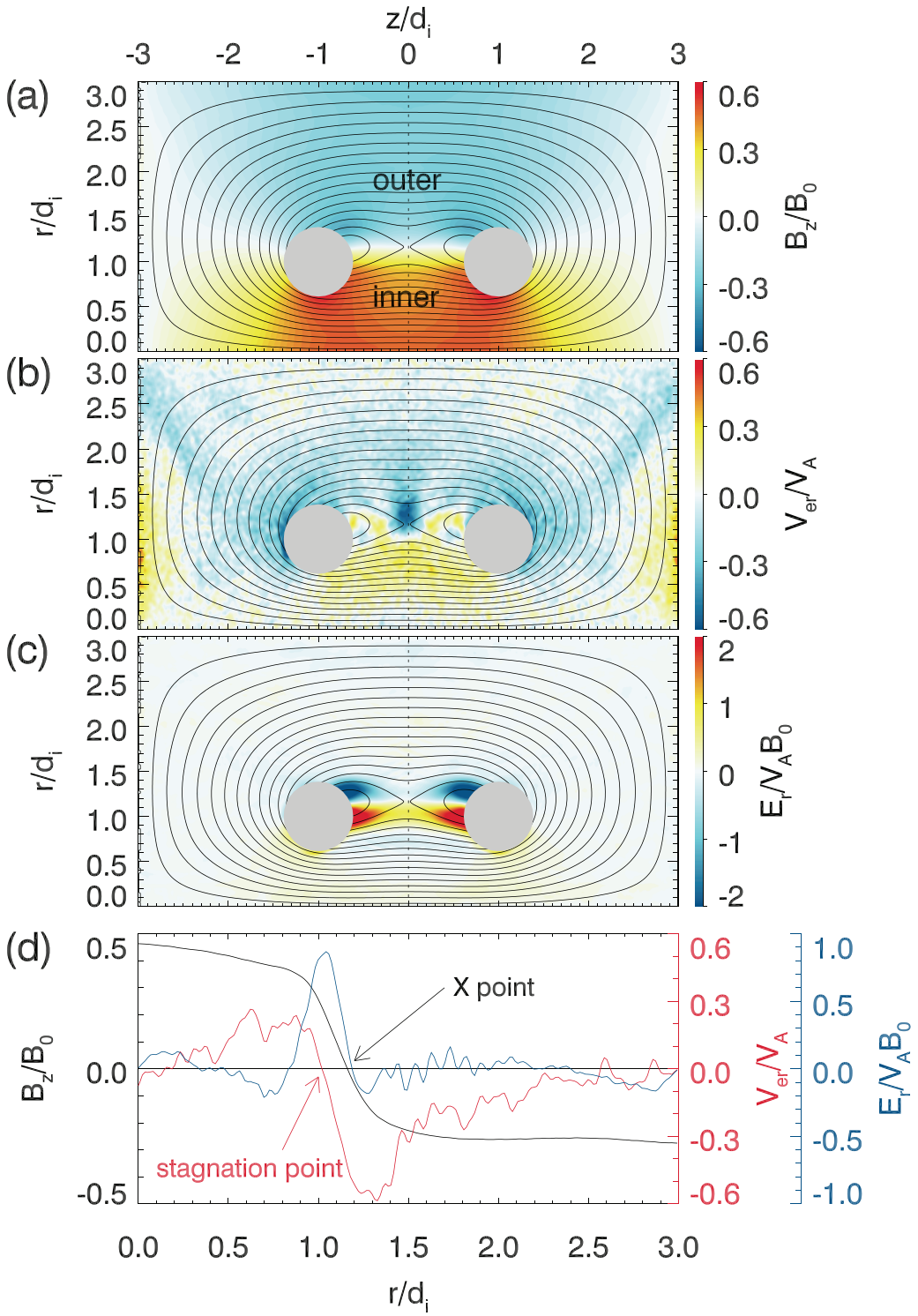

Figure 5. (a) Magnetic field B_z/B_0, (b) electron bulk velocity V_{er}/V_A, (c) electric field E_r/V_AB_0 at $\Omega_i t = 3$. Panel (d) shows the line cut of B_z, V_{er}, and E_r along $z = 0$, the dashed line in panel (a) – (c). The black curves represent the in-plane magnetic field lines. The decay time of the coil current is $\Omega_i T_D = 2$.

where the distribution function is observed becomes farther from the X point, and the density ratio between the crescent component and the core component decreases. It is also consistent with previous simulation studies of asymmetric reconnection [7, 23]. The crescent component is formed due to the meandering motion of electrons near the X point. When these electrons penetrate into the inner inflow region, they are accelerated by the Hall electric field E_r and deflected to the θ direction by B_z [23]. It is believed to be a robust feature that can be observed near the flow stagnation point during asymmetric reconnection [23]. In panels (e) and (f), ions also show a crescent-like velocity distribution. The crescent component of

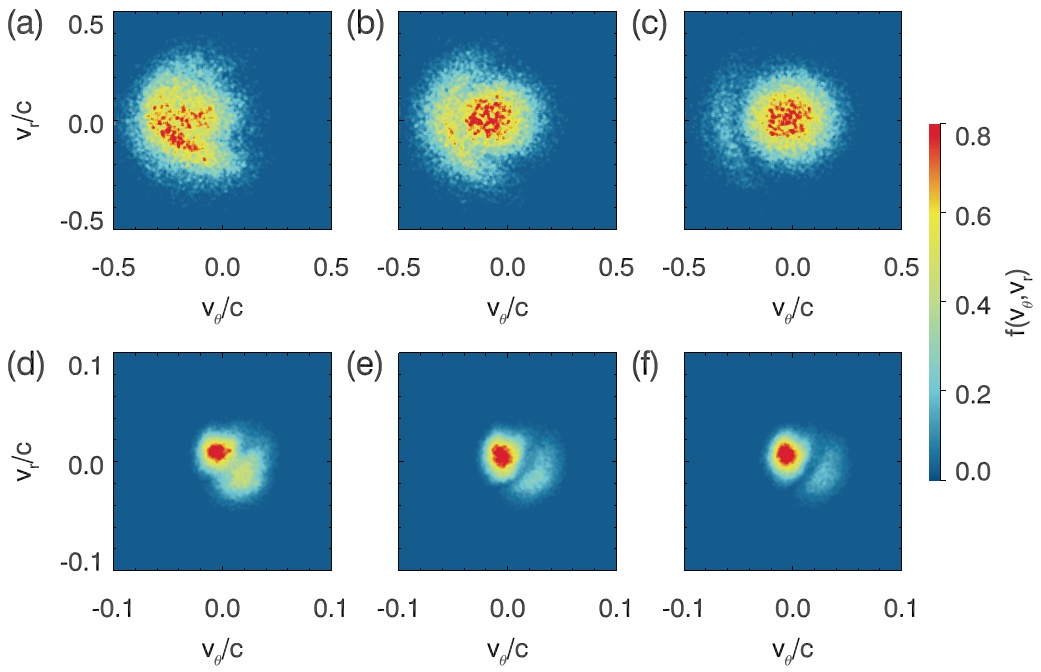

Figure 6. (a)–(c) Electron distribution functions in $v_\theta - v_r$ space at $z/d_i = 0$, $r/d_i = 1.0875$, 1.0125, and 0.9375 respectively, the electrons used to calculate the distribution function are accumulated from a $0.3d_i \times 0.075d_i$ box. (d)–(f) Ion distribution functions in $v_\theta - v_r$ space at $z/d_i = 0$, $r/d_i = 0.825$, 0.675, and 0.525 respectively, the ions used to calculate the distribution function are accumulated from a $0.3d_i \times 0.15d_i$ box. The distribution functions are calculated at $\Omega_i t = 3$ and are integrated over v_z. The decay time of the coil current is $\Omega_i T_D = 2$.

ions has positive v_θ, while the crescent component of electrons has negative v_θ. The reason is that the ion has a different gyro direction from the electron. The ion crescent is observed deeper into the inner inflow region because the ion Larmor radius is larger [24].

The diagnostic of magnetic reconnection and EDR in laser-driven systems is still a big challenge. A proton radiograph can only give an estimation of the topology of the magnetic field [13]. During the contracting of the magnetic bubbles, electrons can be energized through betatron and the Fermi mechanisms, so it is also unclear whether it is reliable to associate the electron heating and power-law distributions with magnetic reconnection [25–27]. Crescent velocity distribution indicates the nongyrotropy and mixture of particles, and therefore it is a more essential feature which is expected to provide a new method of diagnosing reconnection and EDR in laser-driven systems.

The out-of-plane Hall magnetic field is an important feature in collisionless magnetic reconnection [28]. In symmetric antiparallel reconnection, the Hall magnetic field presents a quadrupole pattern. In the ion diffusion region, ion motion is decoupled from the magnetic field while electrons are still magnetized. Electrons are accelerated along the separatrices by the parallel electric field and the magnetic mirror effect [29, 30], forming the electron inflow towards the EDR. After electrons leave the EDR, they will move along the outflow direction and form the electron outflow. Such an in-plane Hall current system carried by electrons is believed to be responsible for the formation of the Hall magnetic field. In asymmetric reconnection, the quadrupole pattern of the Hall magnetic field becomes asymmetric with respect to the current sheet due to the change of the configuration of the Hall current system [31]. Figure 7(a) shows the out-of-plane magnetic field B_θ/B_0 at $\Omega_i t = 1.5$. The distribution of B_θ shows a clear quadrupole signature. The polarity of B_θ is also consistent with previous studies [30]. However, the B_θ patterns in the outer inflow region exist in larger areas, they wrap around the coil and extend to the inner inflow region. Because the magnetic field is stronger in the inner inflow region than that in the outer inflow region, a magnetic mirror configuration is formed with the mirror point in the inner inflow region. Electrons in the magnetic mirror move along the magnetic field lines from the inner inflow region to the outer inflow region. Because the characteristic evolution timescale of the magnetic field is on the order of Ω_i^{-1}, ions have no response to the magnetic mirror effect. As a result, an in-plane Hall current system from the outer inflow region to the inner inflow region is formed, generating the large scale out-of-plane B_θ in the outer inflow region. In the inner inflow region, the Hall current and Hall magnetic field are similar to those in the symmetric antiparallel reconnection. Figure 7(d) shows a sketch of this process, the red arrows represent the direction of the in-plane current, while the blue symbols denote the direction of the out-of-plane magnetic field. Figures 7(b) and (c) show the in-plane current density J_z/en_0V_A and J_r/en_0V_A, and their distributions are consistent with the sketch in panel (d). This asymmetric Hall magnetic field configuration is different from that in previous studies of asymmetric reconnection, and it is a new feature during magnetic reconnection in cylindrical symmetric geometry.

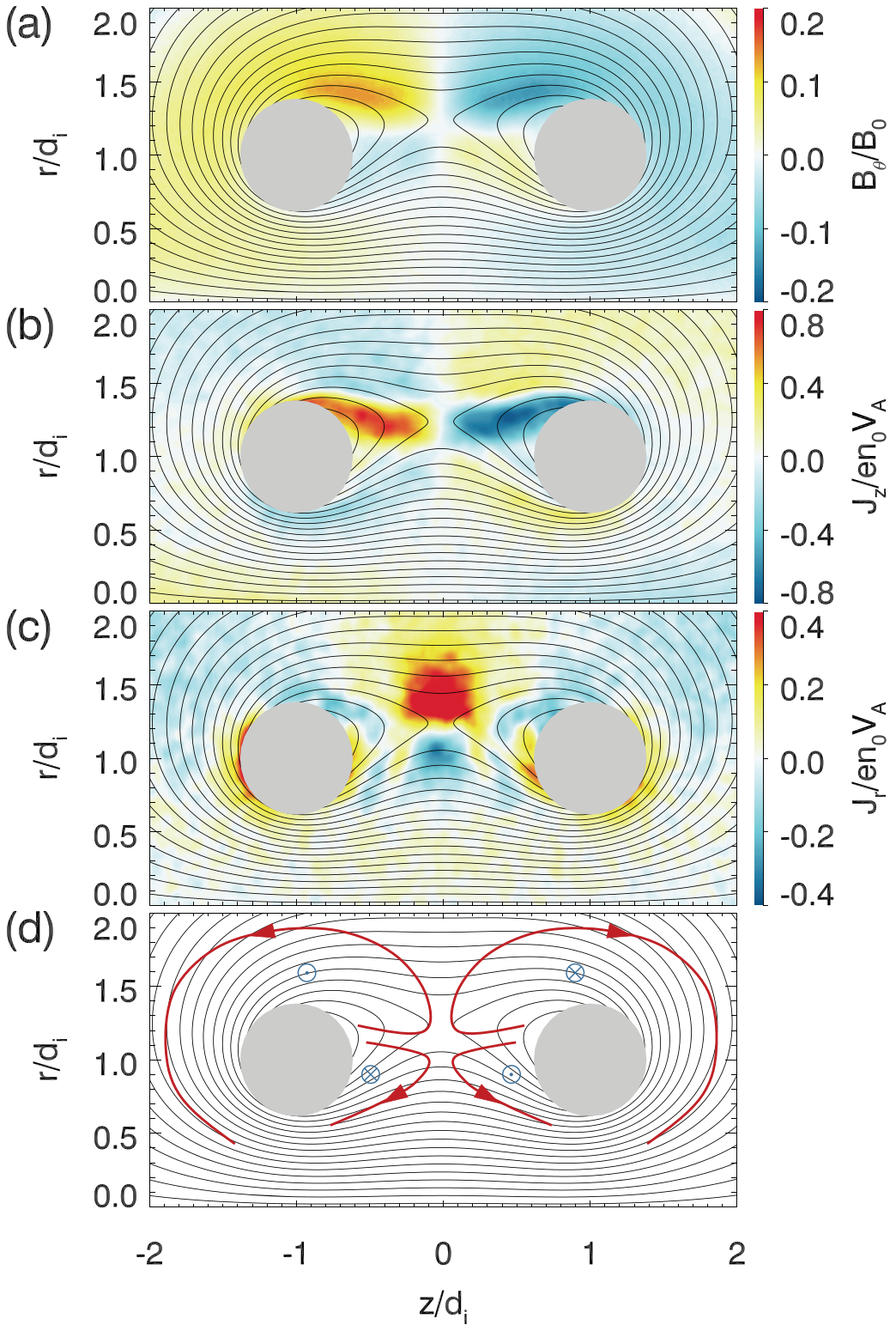

Figure 7. (a) Out-of-plane magnetic field B_θ / B_0, (b) in-plane current density $J_z / en_0 V_A$, (c) in-plane current density $J_r / en_0 V_A$ at $\Omega_i t = 1.5$. Panel (d) is a sketch of the in-plane current and the generated Hall magnetic field. The red arrows show the direction of the in-plane current, while the blue symbols represent the direction of the Hall field. The black curves represent the in-plane magnetic field lines. The decay time of the coil current is $\Omega_i T_D = 2$.

In figure 8, we study the effect of the decay time of the coil current on the reconnection rate. The decay time is chosen to be $\Omega_i T_D = 2$, 4, 6, 8, and 10 respectively. We can find that the peak reconnection rate in the five cases decreases with a longer decay time of the coil current, or weaker drive. In the cases where $\Omega_i T_D = 6$, 8, and 10, the reconnection rate

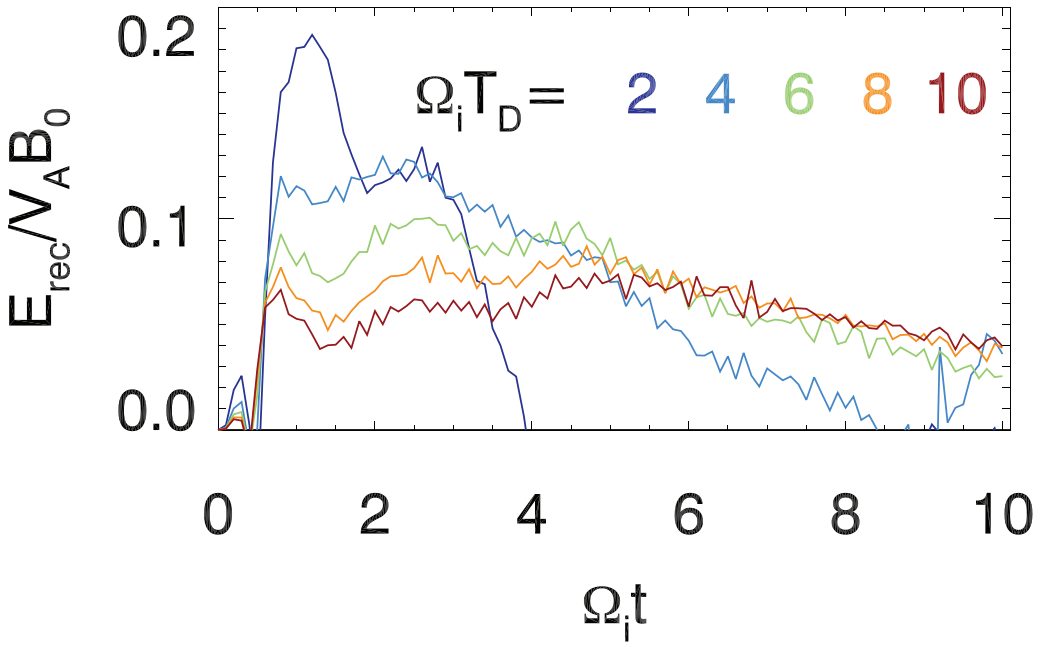

Figure 8. Time evolution of the reconnection rate E_{rec} when the decay time of the coil current is $\Omega_i T_D = 2$, 4, 6, 8, and 10 respectively.

becomes similar after $\Omega_i t \approx 5$; in the cases where $\Omega_i T_D = 2$ and 4, the reconnection rate decreases more rapidly than the other three cases after reaching the peak value. A similar correlation between the peak reconnection rate and the drive time was also shown in the simulation study of reconnection in the magnetic reconnection experiment (MRX) [32]. It should be noted that the increase of the reconnection rate is different from that in the flow driven reconnection in laser-produced plasma, where the large reconnection rate is caused by the increase of the upstream magnetic field due to the squeezing from the plasma motion [33, 34]. In our simulations, there is no obvious enhancement of the upstream magnetic field.

4. Conclusion and discussion

In this paper, 2D PIC simulations are performed on the (z, r) plane in a cylindrical coordinate to study the pull phase of magnetic reconnection driven by a laser-powered capacitor coil. Due to the cylindrical symmetric geometry of reconnection, the reconnecting magnetic field in the outer inflow region is smaller than that in the inner inflow region, leading to the asymmetric performance of reconnection. Many features such as asymmetric inflow speed, asymmetric Hall electric field, separated magnetic null point and flow stagnation point are observed in our simulation, and they are consistent with previous observations and simulations. The peak reconnection rate is around $0.2 V_A B_0$, and it decreases when the drive becomes weaker.

Electron and ion crescent velocity distributions are observed in the inner inflow region where the upstream magnetic field is stronger. The characteristic of the distributions is consistent with previous observations and simulations. We argue that these distributions can be used as evidences for the diagnostic of magnetic reconnection and EDR during the experiments. Thanks to the electron Thomson scattering and laser-induced fluorescence technology, it will be possible to measure the electron and ion distribution functions in a higher spatial and velocity resolution in the near future [35, 36]. Many observations and simulations show that large amplitude upper-hybrid waves and electromagnetic waves can be generated by the crescent velocity distribution of electrons near the EDR [37–39]. These wave activities can provide us with an opportunity to remotely detect the diffusion region during reconnection experiments in laser-produced plasma, as well as magnetic reconnection in solar and astrophysical environments [37].

We find that in the outer inflow region, the Hall magnetic field pattern extends in a larger region around the coil, while in the inner inflow region the Hall magnetic field is similar to that in symmetric antiparallel reconnection. The Hall magnetic field in the outer inflow region is formed due to the decoupled motion between ions and electrons in a magnetic mirror developed in the cylindrical symmetric geometry. This new feature, which is different from previous studies, is expected to be observed in the experiment [40, 41]. Huang *et al* [18] also observed asymmetric Hall magnetic field between the two reconnection outflow regions in such an experiment during the rising phase of the coil current. This asymmetry is formed due to the convergent flow at $r = 0$ in the cylindrical coordinate, and is different from that in the current work.

In our simulations, the spatial scale of the reconnection region is on the ion inertial scale, and the drive time is around the ion gyro period. These conditions are quite similar to those in the studies of electron-only reconnection [42, 43]. Although ion response to the reconnection process is weak in our simulations, it still exists. Therefore, our study shows a transition stage between ion-coupled and electron-only reconnection. In

reality, the mass ratio between ion and electron is much larger than that in our simulations; the experiment can be conducted on a spatial scale much smaller than the ion inertial length but much larger than the electron inertial length. Then it is expected that electron-only reconnection without ion outflow jets can be observed.

Magnetic reconnection driven by laser-powered capacitor coils provides a new platform to experimentally study asymmetric reconnection in the laboratory. It has potential applications in reconnection in the Earth's magnetopause where the plasma beta is around or below one. With the help of PIC simulations, some detailed questions which are difficult to study in the laboratory are addressed, providing guidance for the experiments. The results in this paper are expected to be verified experimentally in the future. In this paper, we use simple initial and boundary conditions, and some parameters like mass ratio are also artificial. Although the results in this work are insensitive to these assumptions, a quantitative comparison with the experimental results needs further study with more realistic boundary conditions and parameters , and this can be carried out in future work.

Acknowledgments

This work was supported by the NSFC Grant Nos. 41527804, 41774169, and Key Research Program of Frontier Sciences, CAS (QYZDJ-SSW-DQC010). A C, L G and H J acknowledge support by the US Department of Energy Office of Fusion Energy Science through High-Energy-Density Laboratory Plasma Science program under Grant No. AWD1006301.

ORCID iDs

Kai Huang https://orcid.org/0000-0003-3630-309X
Hantao Ji https://orcid.org/0000-0001-9600-9963

References

[1] Shibata K and Magara T 2011 *Living Rev. Sol. Phys.* **8** 1
[2] Angelopoulos V *et al* 2008 *Science* **321** 931
[3] Wesson J A 1990 *Nucl. Fusion* **30** 2545
[4] Pe'er A 2015 *Adv. Astron.* **2015** 269
[5] Burch J L *et al* 2016 *Science* **352** aaf2939
[6] Wang R S *et al* 2017 *Phys. Rev. Lett.* **118** 175101
[7] Shay M A, Phan T D, Haggerty C C, Fujimoto M, Drake J F, Malakit K, Cassak P A and Swisdak M 2016 *Geophys. Res. Lett.* **43** 4145
[8] Rosenberg M J, Li C K, Fox W, Igumenshchev I, Séguin F H, Town R P J, Frenje J A, Stoeckl C, Glebov V and Petrasso R D 2015 *Nat. Commun.* **6** 6190
[9] Dong Q L *et al* 2012 *Phys. Rev. Lett.* **108** 215001
[10] Zhong J Y *et al* 2010 *Nat. Phys.* **6** 984
[11] Nilson P M *et al* 2006 *Phys. Rev. Lett.* **97** 255001
[12] Pei X X *et al* 2016 *Phys. Plasmas* **23** 1
[13] Chien A *et al* 2019 *Phys. Plasmas* **26** 062113
[14] Gao L, Ji H T, Fiksel G, Fox W, Evans M and Alfonso N 2016 *Phys. Plasmas* **23** 1012
[15] Fujioka S *et al* 2013 *Sci. Rep.* **3** 1170
[16] Courtois C, Ash A D, Chambers D M, Grundy R A D and Woolsey N C 2005 *J. Appl. Phys.* **98** 054913
[17] Daido H, Miki F, Mima K, Fujita M, Sawai K, Fujita H, Kitagawa Y, Nakai S and Yamanaka C 1986 *Phys. Rev. Lett.* **56** 846
[18] Huang K, Lu Q M, Gao L, Ji H T, Wang X Y and Fan F B 2018 *Phys. Plasmas* **25** 052104
[19] Fiksel G, Fox W, Gao L and Ji H T 2016 *Appl. Phys. Lett.* **109** 846
[20] Yamada M, Ji H, Hsu S, Carter T, Kulsrud R, Bretz N, Jobes F, Ono Y and Perkins F 1997 *Phys. Plasmas* **4** 1936
[21] Lu Q M, Ke Y G, Wang X Y, Liu K J, Gao X L, Chen L J and Wang S 2019 *J. Geophys. Res. Space Phys.* **124** 4157
[22] Malakit K, Shay M A, Cassak P A and Ruffolo D 2013 *Phys. Rev. Lett.* **111** 135001
[23] Bessho N, Chen L J and Hesse M 2016 *Geophys. Res. Lett.* **43** 1828
[24] Lapenta G *et al* 2017 *J. Geophys. Res. Space Phys.* **122** 2024
[25] Drake J F, Swisdak M, Che H and Shay M A 2006 *Nature* **443** 553
[26] Fu X R, Lu Q M and Wang S 2006 *Phys. Plasmas* **13** 012309
[27] Huang K, Lu Q, Huang C, Dong Q, Wang H, Fan F, Sheng Z, Wang S and Zhang J 2017 *Phys. Plasmas* **24** 102101
[28] Eastwood J P, Phan T D, Oieroset M and Shay M A 2010 *J. Geophys. Res. Space Phys.* **115** A08215
[29] Fujimoto K 2014 *Geophys. Res. Lett.* **41** 2721
[30] Lu Q M, Huang C, Xie J L, Wang R S, Wu M Y, Vaivads A and Wang S 2010 *J. Geophys. Res. Space Phys.* **115** A11208
[31] Sang L L, Lu Q M, Wang R S, Huang K and Wang S 2019 *Astrophys. J.* **877** 155
[32] Dorfman S, Daughton W, Roytershteyn V, Ji H, Ren Y and Yamada M 2008 *Phys. Plasmas* **15** 102107
[33] Fox W, Bhattacharjee A and Germaschewski K 2011 *Phys. Rev. Lett.* **106** 215003
[34] Huang K, Huang C, Dong Q, Lu Q, Lu S, Sheng Z, Wang S and Zhang J 2017 *Phys. Plasmas* **24** 041406
[35] Vincent B, Tsikata S, Mazouffre S, Minea T and Fils J 2018 *Plasma Sources Sci. Technol.* **27** 055002
[36] Stark A, Fox W, Egedal J, Grulke O and Klinger T 2005 *Phys. Rev. Lett.* **95** 235005
[37] Graham D B *et al* 2017 *Phys. Rev. Lett.* **119** 025101
[38] Burch J L *et al* 2019 *Geophys. Res. Lett.* **46** 4089
[39] Dokgo K, Hwang K J, Burch J L, Choi E, Yoon P H, Sibeck D G and Graham D B 2019 *Geophys. Res. Lett.* **46** 7873
[40] Yoo J, Na B, Jara-Almonte J, Yamada M, Ji H, Roytershteyn V, Argall M R, Fox W and Chen L-J 2017 *J. Geophys. Res. Space Phys.* **122** 9264
[41] Yoo J, Yamada M, Ji H T, Jara-Almonte J, Myers C E and Chen L J 2014 *Phys. Rev. Lett.* **113** 095002
[42] Phan T D *et al* 2018 *Nature* **557** 202
[43] Pyakurel P S *et al* 2019 *Phys. Plasmas* **26** 082307